Cu-Exchanged Ferrierite Zeolite for the Direct CH4 to CH3OH Conversion: Insights on Cu Speciation from X-Ray Absorption Spectroscopy

(Article begins on next page)

19 April 2024

Cu-Exchanged Ferrierite Zeolite for the Direct CH_4 to CH_3OH Conversion: Insights on Cu Speciation from X-Ray Absorption Spectroscopy.

Dimitrios K. Pappas,[1*] Elisa Borfecchia,[2,3] Kirill A. Lomachenko,[4] Andrea Lazzarini,[1] Emil S. Gutterød,[1] Michael Dyballa,[1,5] Andrea Martini,[6,7] Gloria Berlier,[3] Silvia Bordiga,[1,3*] Carlo Lamberti,[6,7] Bjørnar Arstad,[5] Unni Olsbye,[1] Pablo Beato,[2*] Stian Svelle[1]

[1] Center for Materials Science and Nanotechnology (SMN), Department of Chemistry, University of Oslo, 1033 Blindern, 0315 Oslo, Norway

[2] Haldor Topsøe A/S, Haldor Topsøes Allé 1, 2800 Kongens Lyngby, Denmark

[3] Department of Chemistry, NIS Centre and INSTM Reference Center, University of Turin, via P. Giuria 7, 10125 Turin, Italy

[4] European Synchrotron Radiation Facility, 71 avenue des Martyrs, CS 40220, 38043 Grenoble Cedex 9, France

[5] SINTEF Industry, Forskningsveien 1, 0373 Oslo, Norway

[6] Smart Materials Research Institute, Southern Federal University, Sladkova Street 174/28, 344090 Rostov-on-Don, Russia

[7] Department of Physics, CrisDi Interdepartmental Center and INSTM Reference Center, University of Turin, via P. Giuria 1, 10125 Turin, Italy

e-mail: dimitrios.pappas@smn.uio.no; silvia.bordiga@unito.it; pabb@topsoe.com

Abstract

The direct stepwise transformation of CH_4 to CH_3OH over Cu-exchanged zeolites has been an intensively researched reaction as it can provide a solution for the utilization of this abundant feedstock. Up to date a commercial process is far from realization, which is why an understanding of the Cu speciation in zeolites as a function of reaction conditions as well as the development of a mechanistic view of the reaction are necessary to further advance the field. Herein we study Cu-exchanged Ferrierite zeolite for the direct CH_4 to CH_3OH conversion by utilizing X-Ray Absorption Spectroscopy (XAS), in order to assess the local structure and electronic properties of Cu through the reaction. A Cu-FER sample with a Cu/Al = 0.20 and Si/Al = 11 was subjected to three reaction cycles yielding ultimately 96 $\mu mol_{CH_3OH}/g_{zeolite}$. Normalized to the Cu loading, this accounts for 0.33 mol_{CH_3OH}/mol_{Cu}, making the sample comparable to very active Cu-MOR materials reported in the literature. During O_2 activation, a transient self-reduction regime of Cu^{II} to Cu^{I} ions was identified; eventually leading to mostly framework interacting Cu^{II} species. CH_4 loading leads to a reduction of these Cu^{II} containing species; which are finally partially reoxidized during H_2O-assisted CH_3OH extraction. The speciation after CH_4 activation as well as H_2O-assisted CH_3OH extraction was assessed via Linear Combination Fitting analysis of the XAS data.

Keywords

XAS, Direct CH_4 to CH_3OH Conversion, Cu-Exchanged Ferrierite, Linear Combination Fitting Analysis

1. Introduction

The realization of a process where methane can be transformed into methanol, bypassing the syngas route, can have tremendous impact on the chemical and energy industries, ultimately altering their future. Such a process with ease in implementation and feasibility in small scale can be beneficial economically as well as environmentally by utilizing methane reserves that would be otherwise flared or vented. For the aforementioned reasons, a lot of research efforts have been pointed to that direction by the academia and the industry. Different approaches have been proposed towards this goal; however most of them with certain drawbacks, usually suffering from low conversion and/or too high selectivity towards overoxidation products. Among the direct methane to methanol routes, methane dehydroaromatization, oxidative coupling to hydrocarbons, halogenation, pyrolysis as well as selective partial oxidation constitute the most important ones; though none has been commercially realized [1-4].

One of the most selective systems in combining methane and oxygen to produce methanol at ambient conditions over Cu active centers are the methane monooxygenase enzymes found in nature. In a successful attempt to mimic these biological systems, Cu sites hosted in the confined environment of zeolites have been established as materials that can successfully activate methane [5]. However, the introduction of Cu into the zeolite framework alone does not generate the active Cu configurations; a high temperature activation in the presence of an oxidant is required. For that reason, the methane to methanol conversion has been established as a multistep process, starting with the aforementioned high temperature oxidative treatment (typically over 400 °C) to generate Cu species responsible for the cleavage of the C-H bond in CH_4. The loading of methane conversely requires a lower temperature, in the range of 150 to 350 °C, in order to avoid the overoxidation of methane and to stabilize/protect the activated intermediate in the confined zeolite environment. Finally, the release of CH_3OH is achieved by the introduction of a solvent, commonly water, at a temperature of 200 °C or lower.

The above described multiple step process required to convert CH_4 to CH_3OH over Cu zeolites has been established as a chemical looping system. However, recently alternative approaches have been proposed. The use of H_2O as an oxidant was proposed by Sushkevich et al. [6], where Cu zeolites are activated in anaerobic conditions using H_2O, enabling the formation of active sites [6]. In addition, isothermal approaches of the reaction have been suggested; in one case O_2 activation and methane loading are conducted isothermally at 200 ⁰C and high CH_4 pressure over mostly Cu-MOR zeolites [7-9]. Similarly when using NO as the oxidant the whole process could take place at 150 ⁰C over Cu-ZSM-5 [10].

Nevertheless, both of the latter approaches exploit high-pressure methane loading; which has been shown to enhance the methanol yield and make it comparable to that obtained with high temperature activation. A step beyond the chemical looping system is the catalytic process where the reactants are co-fed over the Cu-zeolite [11,12]. In these cases, the catalysts exhibit catalytic turnovers, producing CH_3OH from CH_4 at a steady state. However, also here the main drawback is the low CH_4 conversion as well as the overoxidation towards CO_2 [11,12].

Up to date different zeolite frameworks have been proposed to be capable of hosting the active Cu species; among them MOR [5-8,13-29], CHA [24,30-35] and MFI [8,10,11,36-41] have exhibited the highest activity for the CH_4 to CH_3OH conversion and thus have attracted a lot of research attention. The efforts aim on one hand to optimize the performance as well as the properties of the materials and

on the other hand, to resolve a long-standing debate on the nuclearity as well as the geometrical configuration of the active sites. Up to date monocopper [26,30,42,43], dicopper [5,15-17,20,25,26,30,32,36,37,43-47] as well as tricopper [18,41,46,48,49] configurations have experimentally and theoretically been demonstrated to exist in the different zeolite frameworks. Higher nuclearity Cu moieties have been only theoretically envisaged [50]. Spectroscopic techniques such as Raman, UV-vis as well as X-Ray Absorption Spectroscopy are the most utilized experimental tools to resolve the Cu species nature and to study the reaction.

In the case of Cu-MOR, the active species have been identified mostly as mono(μ-oxo)dicopper moieties. Recently the effect of Si/Al in the speciation and nuclearity of Cu-species in MOR was addressed by Sushkevich et al., where Al distribution affects the probability of dicopper species formation [26]. In the case of Cu-CHA, where two cationic sites exist with different redox barriers, the Al content has been shown to have an effect on the nature of the Cu species as well as their reactivity. Multimeric moieties such as μ-oxo and peroxo Cu^{II} species are favored at high Al contents (i.e. low Si/Al ratios). In addition, the CHA framework possesses two cationic sites with different binding energy which has been demonstrated to affect the performance of the material at low Cu loadings, showing a preferentiality of Cu towards 2Al6mr (2 Al atoms in a six-member ring) sites. In that position, copper sits as a redox-resistant bare Cu^{II}, hampering the reactivity of the sample [51]. It is therefore evident that the available cationic sites in the frameworks as well as the compositional characteristics of Cu-exchanged zeolites in terms of Si/Al and Cu/Al ratios affect Cu speciation and the activity towards the conversion.

Similarly, to the CHA framework, FER has been reported to possess multiple cationic sites [52-55]. Most studies reported in the literature characterize Cu^I ions in the framework, where three distinct Cu sites have been identified [53-56]. These sites are located in the main (M) 10-member ring (10r) and the perpendicular (P) to 8-member ring (8r) channels, as well as at their intersection (I). The binding energy of Cu^I ions on the wall of both channels was found to be lower compared to in the intersection [54]. Reports on Cu^{II} ions in the FER framework also place these cations in the same sites [52]. Cu-FER zeolites have been investigated also in the past for the direct CH_4 to CH_3OH conversion [11,34,36]. Smeets et al. studied FER with Cu/Al = 0.42 and Si/Al = 6.2 exhibiting a CH_3OH yield of 12 $\mu mol_{CH3OH}/g_{zeolite}$ after overnight activation at 450 °C in 100% O_2 flow and CH_4 loading with 5% CH_4 at 200 °C. Later a sample with Cu/Al = 0.38 and Si/Al = 8.9 exhibited very similar yield of 15 $\mu mol_{CH3OH}/g_{zeolite}$ [34]. However UV-Vis-NIR did not show a distinct band at 22000 cm^{-1}, previously ascribed to bis(μ-oxo)dicopper, leading the authors to conclude that in the case of Cu-FER the active site responsible for the conversion is different than the proposed moieties [36].

Herein we investigate the direct CH_4 to CH_3OH conversion over Cu-exchanged Ferrierite. The sample with Cu/Al = 0.20 was synthesized from the Na-form of FER with Si/Al = 11. Detailed physicochemical characterization was performed to verify the synthesis as well as to determine the compositional characteristics of the sample. Applying reaction conditions and multiple reaction cycles, in order to maximize the active site concentration and thus the CH_3OH yield [51], we obtained a CH_3OH output of 0.33 mol_{CH3OH}/mol_{Cu}. In addition we exploited X-Ray Absorption Spectroscopy (XAS) [57-60] to study the electronic and geometrical characterstics of Cu ions during the stepwise conversion. Time- and temperature-resolved XANES spectra were measured during the key steps of the conversion (O_2 activation, CH_4 loading, H_2O-assisted CH_3OH extraction) along with online MS

data. Static scans in the end of the key steps allowed us to compare the different XANES features of Cu-FER in the direct CH_4 to CH_3OH conversion. Finally Linear Combination Fitting (LCF) analysis enabled the estimation of the fraction of various Cu species after CH_4 loading and H_2O-assisted CH_3OH extraction. The reported results enlighten the understanding of Cu speciation during the conversion over Cu-FER.

2. Experimental

2.1 Synthesis

The parent FER zeolite was purchased from Zeolyst, CP914C (NH_4-FER). Initially the material was calcined in air for 12 h at 550 °C (ramp 1 °C/min) in order to remove any residue. The thus obtained zeolite was then exchanged at 60 °C five times with a solution of $NaNO_3$ (Sigma-Aldrich). The sample was then washed with demineralized H_2O in order to remove the nitrates. The exchange finally resulted in the parent H,Na-FER.

Liquid Ion Exchange (LIE) was conducted using copper(II)acetate from Sigma-Aldrich. The salt was diluted in distilled H_2O resulting in a solution of 0.02 M, and finally the parent material was added to a ratio of 60 (ml liquid)/(g zeolite). A NH_4OH-solution was utilized in order to adjust the pH in the 5.2 – 5.7 range, to avoid Cu precipitation while it was continuously stirred at room temperature for 16h. Solvent was removed via centrifugation and the obtained powder was then washed with H_2O three times to remove excess of Cu ions. The compositional characteristics as well as results from N_2 physisorption measurements can be found in **Table 1** in **Sect. 3.1**.

2.2 Laboratory Physico-Chemical Characterization

N_2-physisorption at 77K was measured in a BELSORP-miniII instrument. The samples were treated in vacuum at 80 °C and 300 °C for 1 h and 2 h respectively. Using the Brunauer-Emmett-Teller (BET) equation [61] we calculated the specific surface area. Scanning Electron Microscopy (SEM) images were taken on a Hitachi SU8230 instrument. Energy-Disperse X-ray (EDX) spectroscopy at 20 kV accelerating voltage was used to determine the elemental composition of the materials on 200x200 μm areas, while quantification was performed with Bruker Quantax system consisting of a XFlash 6T|10 detector and Espirit. Thermogravimetric Analysis (TGA) was utilized to calculate the H_2O content of the zeolites by heating the sample to 300 °C (ramp 1 °C /min). The H_2O content was used for the correction of sample mass during the quantification of the conversion products. X-ray Diffraction (XRD) patterns were collected on a Bruker D8 Discovery diffractometer using Cu-Kα radiation (λ = 1.5418 Å) in a 2θ range from 2 to 70° in Bragg-Brentano geometry. ^{27}Al NMR spectra were collected using a Bruker Avance III spectrometer (at 11.74 T) using a 4 mm double resonance probe at a MAS rate of 10 KHz.

2.3 Activity in the Direct Stepwise CH_4 to CH_3OH Conversion Tests

The activity of the synthesized Cu-exchanged zeolite in the direct CH_4 to CH_3OH conversion was tested in a quartz fixed bed reactor (I.D. = 6 mm), at ambient pressure. Prior to the measurements

the powders were pressed, ground and sieved in order to get a particle distribution in the range of 425-250 μm. The temperature of the zeolite bed was controlled using a tubular oven, monitored by a thermocouple inserted in the middle of the packed sample. All the flows were controlled using Mass Flow Controllers (MFC) and remained constant at 15 ml/min total flow.

The reaction proceeds as described schematically in **Fig. 1**. Initially the samples were dried in helium flow (15 ml/min) at 150 °C; then O_2 flow (100%, 15 ml/min) was introduced and the temperature was increased (ramp 5 °C/min) to 500 °C. The temperature was kept at 500 °C for 480 min; afterwards with the same ramp the temperature was decreased to 200 °C, keeping the O_2 flow. After reaching 200 °C the sample was purged with He for 60 min before CH_4 was introduced. CH_4 loading took place also at 200 °C by flowing 15 ml/min of CH_4 (100%) for 360 minutes. Finally, the sample was purged again with He for 60 min before the isothermal online extraction of CH_3OH with 15 ml/min 10% H_2O steam; the effluent was analyzed by an online Mass Selective Detector (MSD) (Hewlett Packard 6890/5972 GC-MS). CH_3OH, CH_3OCH_3 and CO_2 were the main products detected (CH_3OCH_3 was accounted as two CH_3OH molecules).
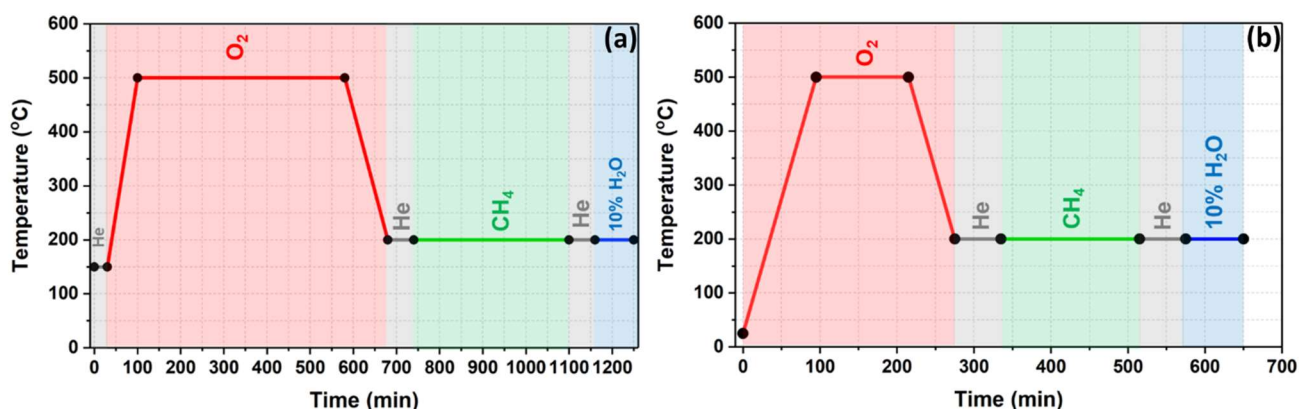

Fig. 1 Schematic representation of the stepwise CH_4 to CH_3OH conversion using (a) reference reaction conditions and (b) XAS measurements conditions. The x-axis represents the time for each step in minutes while the y-axis reports the temperature in °C; the color-coded segments represent the different flows used during the experiment. In detail for the reference reaction conditions (a) 480 min O_2 activation at 500 °C (red), 360 min CH_4 loading at 200 °C (green), steam-assisted CH_3OH extraction at 200 °C for ca. 60 min (blue). Helium flushing (grey segments) was performed after O_2 activation and CH_4 loading for ca. 60 min the cooling/heating ramps are performed in the same rate of 5 °C/min. For XAS conditions (b) 120 min O_2 activation at 500 °C (red), 180 min CH_4 loading at 200 °C (green), steam-assisted CH_3OH extraction at 200 °C for ca. 60 min (blue). Helium flushing (grey segments) was performed after O_2 activation and CH_4 loading for ca. 60 min.

2.4. X-ray Absorption Spectroscopy (XAS)

XAS data during the direct CH_4 to CH_3OH conversion over 0.20Cu-H,Na-FER(11) were collected at the BM31 beamline [62] of the European Synchrotron Radiation Facility (ESRF, Grenoble, France). The reaction protocol followed in the case of the XAS experiments is depicted in **Fig. 1a**. A 1 mm diameter quartz capillary, with the powdered sample placed between glass wool plugs, was fixed in a metal bracket and was used as a fixed bed reactor. For the measurement 3 mg of the 0.20Cu-H,Na-

FER(11) were used. The inlet was connected to a dedicated gas flow setup, while the outlet to an online MS (Pfeiffer Vacuum). The temperature of the sample was controlled using a heat gun and the heating/cooling ramps were performed with a 5 °C/min rate. The flow at each step was set to 2 ml/min using dedicated MFCs. As discussed above the process consists of three main steps, however in the case of the XAS experiments the duration was decreased. In detail, O_2 activation at 500 °C (120 min, 100% O_2), CH_4 loading at 200 °C (180 min, 100% CH_4), and H_2O-assisted CH_3OH extraction at 200 °C (ca. 60 min). The steam-assisted extraction was performed by saturating a 10% Ar/He flow through DI H_2O at 44 °C. Finally, the effluent was analyzed by the MS where CH_3OH (m/z = 31), CH_3OCH_3 (m/z = 46) CO_2 (m/z = 44) were the main products of the reaction (CH_3OCH_3 was accounted as two CH_3OH molecules for products quantification)

Cu K-edge XAS spectra were collected in transmission mode, using a water-cooled flat-Si (111) double crystal monochromator. The incident (I_0) and transmitted (I_1) X-ray intensities were detected using 30 cm long ionization chambers filled with He/Ar mixture. Scans in the range of 8800 – 9300 eV were continuously collected, binned with a constant energy step of 0.5 eV with the acquisition time being ca. 5 min/scan. At the end of each key reaction step two longer scans in the 8800 – 10000 eV range were collected (ca. 10 min/scan). The XAS spectra were normalized to unity edge jump using Athena software from the Demeter package [63].

2.5 XAS Linear Combination Fit (LCF) analysis

Linear combination fit (LCF) [64,65] analysis of final XANES spectra (CH_4 loading and H_2O-assisted CH_3OH extraction steps) was performed in the 8970 – 9020 eV energy interval, using the Athena software from the Demeter package [63]. Based on our experience of XAS experiments on Cu-zeolites [28,30,51,66-71] the XANES spectra were analysed using the three reference spectra representative of pseudo-octahedral Cu^{II} aquo complexes (*Cu^{II} hydr.*) as well as framework interacting Cu^{II} and Cu^I species, referred to as *Cu^{II} fw* and *Cu^I*, respectively. *Cu^{II} hydr.* was obtained by measuring a Cu^{II} acetate aqueous solution at RT. *Cu^I* reference was obtained by heating at 400 °C in vacuum the 0.20Cu-H,Na-FER(11) while the spectra where collected at room temperature with the material still kept in vacuum inside an *ad hoc* cell; this measurement was carried out at BM23 beamline of the ESRF [72], acquisition parameters being equivalent to those used at BM31 beamline. The XANES collected in He at 200 °C (after O_2-activation at 500 °C, cooling to 200 °C in O_2 and flushing the system with He) just before the CH_4 loading step was used was used as *Cu^{II} fw* reference. In order to verify the validity of the *Cu^I* reference, i.e. vacuum activated 0.20Cu-H,Na-FER(11) at 400 °C, the LCF analysis was also performed using $[Cu^I(NH_3)_2]^{2+}$ as the *Cu^I* reference; the obtained fits and results are illustrated in **Fig. S2** in the Supporting Information (SI).

The experimental XANES, $\mu^{EXP}(E)$, was fitted as a linear combination of the three reference XANES spectra, $\mu_i^{REF}(E)$, using: $\mu^{LCF}(E) = \Sigma_i w_i \mu_i^{REF}(E)$, optimizing the weights (w_i) for each reference spectrum. For each analysed scan, the corresponding LCF R-factor was computed as $\Sigma_j [\mu^{EXP}_j(E) - \mu^{LCF}_j(E)]^2 / \Sigma_j [\mu^{exp}_j(E)]^2$, where *j* denotes each experimental point in fitted energy range, (8970 − 9020) eV; R-factor = 0 means the ideal reproduction of the measured spectrum: $\mu^{EXP}(E) \equiv \mu^{LCF}(E)$.

3. Results and Discussion

3.1. Physico-chemical Characterization

The sample names, compositional characteristics as well as the BET total surface area and micropore volume of the parent and the exchanged Cu-zeolite are listed in detail in **Table 1**. From the compositional results obtained from EDX the Cu/Al was equal to 0.20 corresponding to 1.86 wt.%. It should be noticed that prior to Cu exchange the Na/Al ratio of the parent sample was 0.4 and it reaches a value of 0.16 after introduction of Cu. It appears that the presence of Na facilitates the Cu exchange and Na is exchanged with Cu during LIE. From the N_2-physisorption measurements it can be concluded that the surface area as well as micropores volume are maintained after the introduction of Cu.

Table 1 Compositional characteristics and results from N_2-physisoprtion measurement for the parent and the Cu-exchanged samples

	Si/Al ratio[1]	Cu/Al ratio[1]	Na/Al ratio[1]	Cu [wt.%][1]	BET [m²/g]	V_{tot} [ml/g][2]	V_{micro} [ml/g]
H,Na-FER	11	-	0.40	-	422	97	0.24
0.20Cu-H,Na-FER	11	0.20	0.16	1.9	356	82	0.22

1 determined by EDX

2 determined at p/p0 = 0.99

^{27}Al MAS NMR spectroscopy was applied to assess the extra-framework Al content of the samples (**Fig. 2**) [73-76]. The feasibility of this method used in the interpretation of the framework of copper exchanged zeolites used for CH_4 to CH_3OH conversion was evaluated recently [29]. Peaks are interpreted according to common literature [77,78]. Both samples exhibit an intense peak at 55.5 ppm assigned to tetrahedrally coordinated framework aluminum (Al_f). In addition, a minor peak around 0 ppm, appearing after calcination of the NH_4-FER parent at 550 °C, and corresponding to octahedrally coordinated extra-framework aluminum species (Al_{ef}) is present. Furthermore, a high-field shoulder of the peak at 55.5 ppm is attributable to aluminum in distorted tetrahedral or pentahedral coordination.
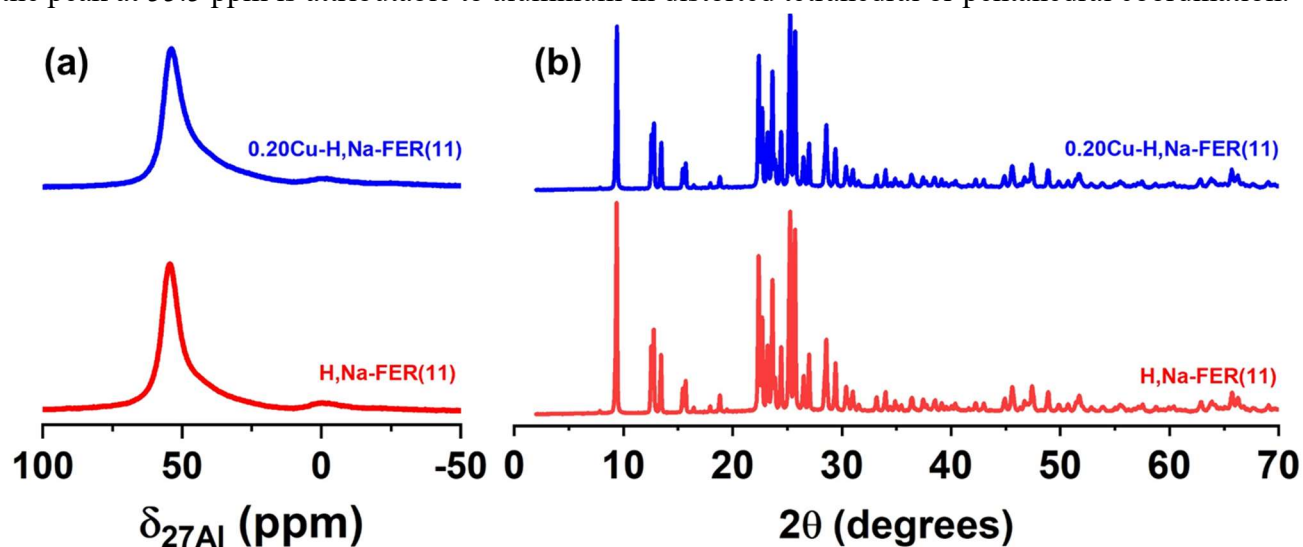
Fig. 2(a) ^{27}Al MAS NMR spectra and **(b)** XRD patterns of the parent (H,Na-FER(11)) and Cu-exchanged (0.20Cu-H,Na-FER(11)) samples.

XRD patterns (**Fig. 2b**) as well as SEM and BSE (**Fig. S1**) images were collected in order to verify the structural integrity of the material as well as the absence of bulk Cu nanoparticles. Indeed, peaks corresponding to CuO are not seen in the diffractograms of the 0.20Cu-H,Na-FER(11). Also, no large bright spots were observed in **Fig. S1b,** where the BSE image is shown. However, small scarce bright spots were observed indicating the presence of few nanoparticles with a maximum size of 50 nm. The contribution of these minor aggregates over the total Cu can be neglected since in the obtained XAS spectra no traces of metal Cu or bulk-like CuO were observed.

3.2. Direct CH_4 to CH_3OH Conversion

The Cu-exchanged sample (0.20Cu-H,Na-FER(11)) was evaluated with respect to its activity in the direct CH_4 to CH_3OH conversion. The reaction protocol followed is described in **Sect. 2.3** and in **Fig. 1** above. The CH_3OH yield in $\mu mol_{CH3OH}/g_{zeolite}$ and mol_{CH3OH}/mol_{Cu} as well as the selectivity (%) are tabulated in **Table 2**. The sample in the first reaction cycle produces 89 $\mu mol_{CH3OH}/g_{zeolite}$ of CH_3OH, which corresponds to 0.30 mol_{CH3OH}/mol_{Cu}. Indeed comparing this value to what is reported to date in the literature [34,36,79], the activity reported here is the highest. However, this can be attributed most probably to the reaction conditions applied here i.e. prolonged O_2 activation at 500 °C as well as CH_4 flow for 360 min with 100% CH_4. Such conditions have been proven before to significantly enhance the methanol yield of Cu-CHA [30].

In addition, the sample was evaluated over multiple reaction cycles in order to address their effect on the material as well as reusability. From the tabulated data (**Table 2**) it can be observed that moving to the second reaction cycle produces a 7 $\mu mol_{CH3OH}/g_{zeolite}$ increase with respect to the first one. An additional reaction cycle does not further impact the productivity of the material. The selectivity at each reaction cycle remains constant around 89%. The yield increment observed has been proposed to be linked to the mobility of hydrated Cu ions, deriving form the final H_2O-assisted extraction step, which migrate to different and more active positions [21,30,66].

Table 2 Direct CH_4 to CH_3OH Conversion Testing Results over 0.20Cu-H,Na-FER(11)

	CH_3OH ($\mu mol_{CH3OH}/g_{zeolite}$)	CO_2 ($\mu mol_{CO2}/g_{zeolite}$)	mol_{CH3OH}/mol_{Cu}	Selectivity (%)
Cycle 1	89	11	0.30	89
Cycle 2	96	13	0.33	88
Cycle 3	96	13	0.33	88

3.3. X-Ray Absorption Spectroscopy over 0.20Cu-H,Na-FER(11)

3.3.1. O_2 Activation

The O_2 activation is the first step of the process and is responsible for the generation of active Cu_xO_y moieties [28,30,32,35,37,39]. XAS was used to track the changes in Cu oxidation and coordination state. The XANES spectra depicted in **Fig. 3** were collected during the heating in O_2 flow

(2 ml/min) from 25 to 500 °C and at the end of O_2 activation at 500 ºC after 120 min (red line **Fig. 3a**). The characteristic XANES features of Cu zeolites are apparent in the figure and can be interpreted based on the Cu K-edge XAS literature on these systems [6,16,18,21,24-26,57,67-69,80,81]. At room temperature Cu exists as hydrated Cu^{II} ions; this is evident by the high White Line (WL) intensity as well as the smooth rising edge. Increasing the temperature, a decrease in the WL intensity is observed along with the evolution of the rising edge peak at 8986 eV. These are the result of dehydration of the sample and the consecutive formation of framework-coordinated Cu^{II} species. In order to obtain a holistic view on the O_2 activation process, the ion intensities of H_2O (m/z = 18), CO_2 (m/z = 44) and CO (m/z = 28) were followed by an online MS and the results are plotted in **Fig. 3b**. As the WL intensity decreases in intensity, the release of H_2O is observed in **Fig. 3b**, evidencing the loss of H_2O ligands from the Cu ions [67,68].

Interestingly, before the H_2O is completely released from the framework, the evolution of CO_2 is observed (at around 250 ºC) in the online MS response (**Fig. 3b**). In the same temperature range the evolution of the peak at 8983 eV (corresponding to the 1s → 4p transition of Cu^I ions) as well as the intensity decrease and shape change of the WL are observed. After further increment of the temperature the 8983 eV peak is decreasing again and the WL is restored, indicating the transient nature of the phenomenon [24]. Herein, combining time/temperature resolved XANES with online MS, we can propose that the transient reduction might be linked to the combustion of hydrocarbon residues from the Cu-exchange in the sample during high temperature activation in an O_2 rich atmosphere, giving rise to CO_x species. Recently, the self-reduction (or autoreduction) of Cu zeolites has been revisited by Sushkevich et al. [82], where the authors conclude that the reduction of Cu in a He atmosphere is attributed to the interaction of Cu with carbonaceous deposits as well as the Cu species "self-reduction". From our data it is not possible to solely link the origin of this transient reduction to the formation of CO_2 and H_2O as products of hydrocarbon oxidation. Indeed, we also observe the release of H_2O at low temperature, which can be related to desorption of physisorbed water and removal of OH ligands from Cu-OH species. In both cases reactive Cu^I species with a low coordination environment are formed, which are possibly precursors for multinuclear Cu_xO_y species. The H_2O signal as depicted in **Fig. 3** displays a plateau at the same time as CO_x peaks appear, evidencing the binary nature of the phenomenon.

Reaching 500 °C only minor modifications in the shape of the WL peak as well as the rising edge features are observed even after activation for 120 min. The final state of the sample in the end of the O_2 activation at 500 °C consists solely of Cu^{II} containing species.
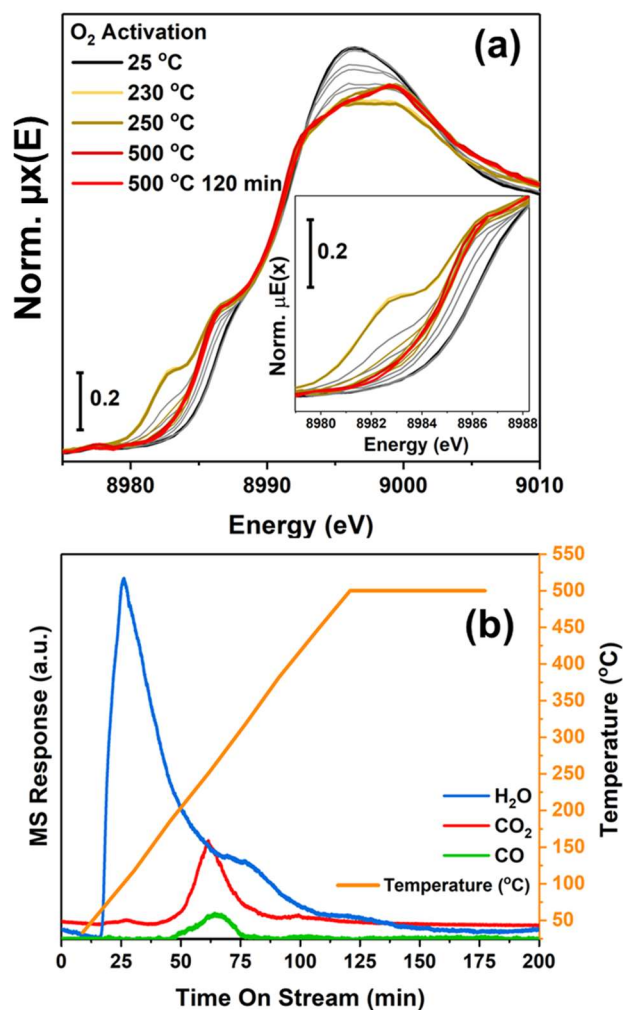
Fig. 3 (a) Cu K-edge XANES spectra of 0.20Cu-H,Na-FER(11) sample during O_2 activation from 25 to 500 °C as well as after 120 min at 500 °C (red thick line). The inset in **Fig. 3a** magnifies the energy region corresponding to the 1s → 4p transitions of Cu^I ions. **(b)** MS response (left axis) during the O_2 activation as well as the temperature profile (right axis); the masses corresponding to H_2O (m/z = 18), CO_2 (m/z = 44) and CO (m/z = 28) were followed during the experiment.

3.3.2 CH₄ Activation & H₂O-Assisted CH₃OH Extraction

The CH_4 loading and H_2O-assisted CH_3OH extraction were also followed: the XANES spectra collected during these steps are depicted in **Fig. 4a** and **Fig. 4b** respectively. In addition, **Fig. 4c** illustrates the collected data from the online MS measurements during the extraction of CH_3OH.

The first scan during CH_4 loading at 200 °C, collected after cooling from 500 °C to 200 °C followed by helium flushing for 60 min, retains the characteristic XANES features of the O_2 activated material. However, a detailed comparison of XANES features of the individual steps is performed in the following section. Upon interaction of the 0.20Cu-H,Na-FER(11) with CH_4 the evolution of the peak corresponding to Cu^I ions is evident, as the intensity of the peak at 8983 eV is developing with reaction time. The Cu^I component generated during CH_4 loading has been well evidenced for other zeolites such as Cu-CHA [24,30] and Cu-MOR [6,25,28] and has been directly linked to the CH_3OH productivity of the materials [6,25,27]. Indeed, based on the literature and mechanism proposed for the

formation of methyl intermediates, where O_{ef} from the Cu_xO_y active species is donated to the methoxy intermediate, we propose that also here the evolution of the peak at 8983 eV is linked to the amount of activated methane. Interestingly, along the intensity increase of the peak at 8983 eV, a decrease in the WL intensity is observed, suggesting that the newly formed Cu^I species possess a lower coordination number [24,67,68]. The development of the Cu^I component does not stabilize in the reaction time of 180 min applied; this indicates that a saturation of the active sites is unlikely at these conditions. CH_4 loading time has been exhibited to impact the productivity of the materials [24,27,30,51] which is also evident by the measured productivity at the XAS experimental conditions (13 $\mu mol_{CH3OH}/g_{zeolite}$) compared to the reference conditions (89 $\mu mol_{CH3OH}/g_{zeolite}$), where increased activation and reaction times were applied.

The final step of the process is, as described above, the H_2O-assisted CH_3OH extraction. The spectra collected during that step as well as the online MS data are depicted in **Fig. 4b** and **Fig. 4c** respectively. From the XANES spectra in **Fig. 4b** the decrease of the Cu^I peak at 8983 eV can be observed along with the progressive increase of the WL intensity. Introduction of H_2O in the sample facilitates the release of the adsorbed intermediate in the form of oxygenates, along with the re-oxidation of Cu species and the hydration of the zeolite. However, even after ca. 60 min on stream the sample did not completely change oxidation state from Cu^I to Cu^{II}, since a small bump at 8983 eV still remains indicating the incapability of H_2O to fully re-oxidize the sample at that temperature. Nevertheless, the extraction time was sufficient to desorb the reaction intermediates as products, as evident from the stabilization of the MS response after 60 min.
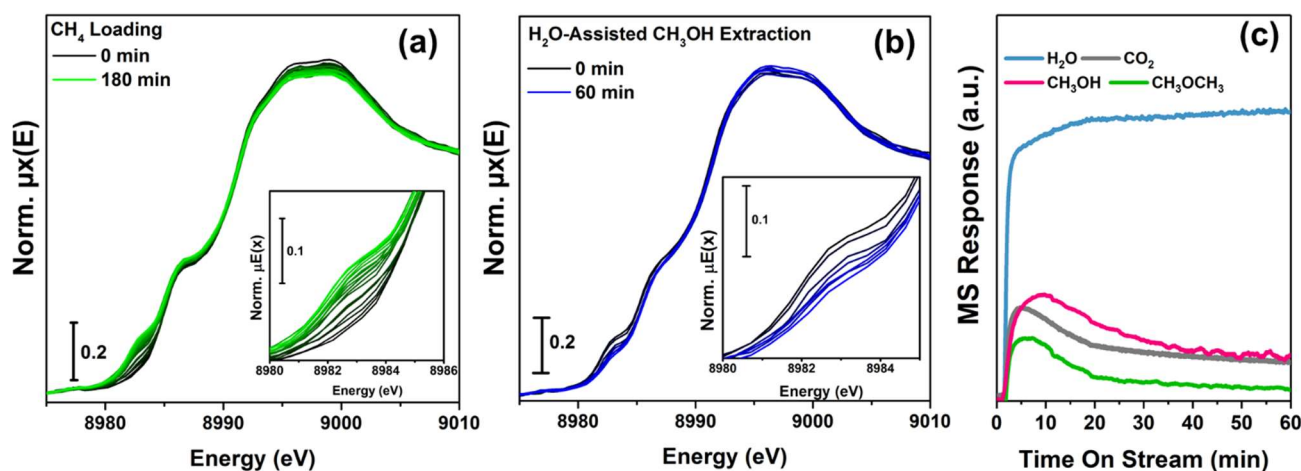

Fig. 4 Cu K-edge XANES spectra of 0.20Cu-H,Na-FER(11) sample during **(a)** CH_4 loading for 180 min and **(b)** H_2O-assisted CH_3OH extraction. The insets in **Fig. 4a** and **Fig. 4b** magnify the energy region corresponding to the 1s → 4p transitions of Cu^I ions. **(c)** MS response during the H_2O-assisted CH_3OH extraction; the masses corresponding to H_2O (m/z = 18), CH_3OH (m/z = 31), CH_3OCH_3 (m/z = 46) and CO_2 (m/z = 44) were followed during this step.

3.3.3. Comparison of Key Reaction Steps

As already discussed in the experimental section, at the end of each reaction step two longer scans were collected and averaged. Herein, these spectra collected during the complete cycle of CH_4 to

CH$_3$OH conversion over 0.20Cu-H,Na-FER(11) will be discussed (**Fig. 5**), including: 1) O$_2$ activation at 500 °C, 2) O$_2$ activated sample cooled at 200 °C, 3) He flush after O$_2$ at 200 °C, 4) CH$_4$ loading at 200 °C and 5) H$_2$O assisted CH$_3$OH extraction at 200 °C. As it will be addressed in more detail from XANES analysis, several Cu-species are simultaneously present in the material during the whole MTM process.
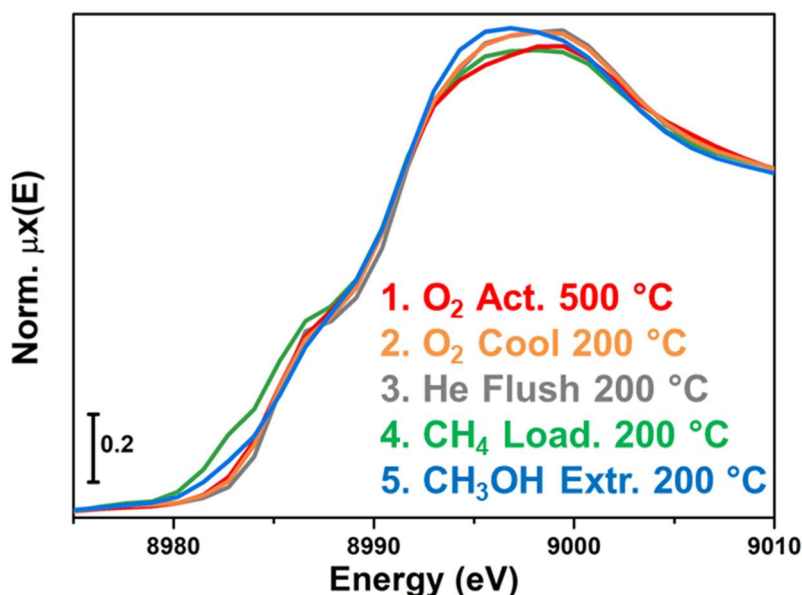

Fig. 5 Cu K-edge XANES spectra and for the key steps of the CH$_4$ to CH$_3$OH conversion over 0.20Cu-H,Na-FER(11).

After O$_2$ activation of 0.20Cu-H,Na-FER(11), which was discussed in **Sect. 3.3.1**, the sample is cooled down in O$_2$ flow. The corresponding spectra are given in **Fig. 5** (red and orange line) and show very similar XANES features, proving that the oxidation state of Cu during the cooling is maintained. Nevertheless, an increased WL intensity is observed for the sample at lower temperature, which suggest that the average coordination number is increased after cooling the sample. In line with previous findings for Cu-CHA [30], these results are consistent with a structural rearrangement of Cu species induced by the decrease in temperature. When the sample is flushed in He, at 200 °C, the collected XANES spectra are almost identical to the O$_2$-activated sample at the same temperature (grey line in **Fig. 5**), indicating an unaltered oxidation state and coordination environment in both conditions.

After interaction of the O$_2$-activated 0.20Cu-H,Na-FER(11) with CH$_4$ at 200 °C for 180 min we observe the partial reduction of Cu^{II} to Cu^{I} indicated by the development of the peak around 8983 eV, which is assigned to the 1s → 4p transition of Cu^{I} ions, together with a suppressed WL intensity. The reduction of Cu^{II} to Cu^{I} during CH$_4$ loading is in agreement with the formation of a reaction intermediate i.e. methoxy species, as suggested in the literature [6,16]. Recently, the percentage of reduced Cu from the interaction of active sites with CH$_4$ has been taken as a descriptor of the productivity [6,25,27]

In order to assess in more detail the Cu speciation after the CH$_4$ loading step, a LCF analysis of the XANES spectra reported in **Fig. 5** was applied as described in **Sect. 2.5**. The results are shown in

Fig. 6a and reveal that interaction of the sample with CH_4 results in 18% framework interacting Cu^I species. The rest of the Cu in the sample remains as Cu^{II} *fw*, while no Cu^{II} *hydr.* species were detected. In order to verify the choice of the Cu^I reference as described in **Sect. 2.5** and illustrated in **Fig. S2**, the LCF analysis was also performed using $Cu^I(NH_3)_2$ as Cu^I reference to assess the uncertainty of the exact shape of the spectrum of Cu^I species formed after CH_4 loading as further discussed in the **SI**.

Finally, the introduction of steam in the reactor in order to release CH_3OH, results in a slight increase of the WL intensity as well as a small modification in its shape, pointing to hydration phenomena involving a fraction of the Cu ions (blue line in **Fig. 5**) [30]. These findings are in agreement with the results obtained from LCF analysis (**Fig. 6b**), namely the formation of Cu^{II} *hydr.* species corresponding to aquo-complexes, accounting for 32% of the total Cu.

The aforementioned oxidation of Cu^I to Cu^{II} is calculated to 5%, while 13% of the total Cu remain as Cu^I. This means that 27% of Cu^{II} *hydr.* is formed at the expense of Cu^{II} *fw*. Comparing the LCF analyses with the different Cu^I references (**Fig. 6** and **Fig S2**) using $Cu^I(NH_3)_2$ as Cu^I reference in this case does not provide an equally good fit (R-factor = $2.8 \cdot 10^{-5}$) compared to using the reduced sample as Cu^I reference (R-factor = $1.9 \cdot 10^{-4}$). However, for both steps the two LCF analyses follow the same trends for the Cu speciation.

From the quantification of the MS data collected during the XANES experiment (**Fig. 4c**) under the specific conditions (**Fig. 1b**) the yield was 13 $\mu mol_{CH3OH}/g_{zeolite}$ or 0.044 mol_{CH3OH}/mol_{Cu}. Interestingly, the productivity closely correlates to the fraction of Cu^I that is reoxidized during steam treatment i.e. 5%. In addition, the productivity normalized to mol of Cu is almost three times lower than the Cu^I fraction after CH_4 loading which is in line with the presence of CO_x species among the products (**Fig. 4c**) [6,25]. This is an indication that the species responsible for the selective CH_4 conversion could be the ones that are re-oxidized during the CH_3OH extraction step, as also previously observed for Cu-CHA [30], Conversely, taking into account the total Cu^I fraction after CH_4 loading, this includes both selective and non-selective sites since different number of electrons are required to produce CH_3OH and CO_x [6,25].
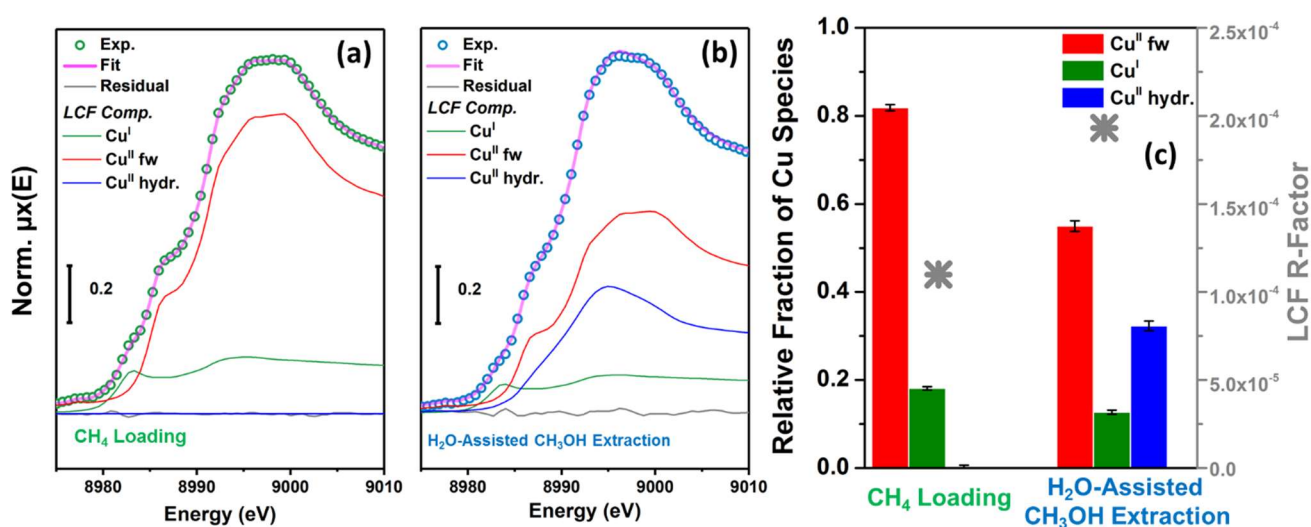

Fig. 6 LCF analysis obtained for **(a)** CH_4 loading and **(b)** H_2O-assisted CH_3OH extraction steps; the experimental spectra (coloured circles), the fit (purple line) the residual (grey lines) as well as the

weighted reference spectra of $Cu^{II} fw$ (red line), Cu^{I} (green line) and $Cu^{II} hydr$. are illustrated in both figures. **(c)** Bar plot of the relative fraction of Cu species for the two fits along with the error bars (left ordinate axis). The R-factor is reported in the right axis (grey stars, right ordinate axis).

4. Conclusions

In this work, we employed XANES in order to elucidate the direct stepwise conversion of CH_4 to CH_3OH over Cu-FER. The material was synthesized by LIE of the H,Na-FER(11) parent zeolite with copper(II)acetate, obtaining a Cu/Al ratio of 0.20. Fixed bed reactor testing, utilizing a long reaction protocol in order to exploit the productivity potential, revealed that the sample can yield up to 89 $\mu mol_{CH3OH}/g_{zeolite}$ with 89% selectivity. A yield increment was observed after the first reaction cycle; at the third and final cycle the sample yielded 96 $\mu mol_{CH3OH}/g_{zeolite}$; normalizing the yield to the Cu concentration results in 0.33 mol_{CH3OH}/mol_{Cu}, making the sample comparable to highly active Cu-MOR zeolites.

For the first time Cu-FER was studied for the CH_4 to CH_3OH conversion. The average local structure and electronic properties of Cu in the framework were revealed by *in situ* XANES in combination with LCF analysis. During heating from RT to 500 ºC in O_2 we identified a transient reduction of Cu^{II} ions, attributing it to the oxidation of hydrocarbon residues and release of O-containing ligands, and possibly related to the formation mechanism of active Cu_xO_y species. During activation, the rearrangement of the local coordination environment and siting of framework-coordinated Cu^{II} ions is also observed. Cooling down to reaction temperature further rearrangement is evident. Interaction of the activated sample with CH_4 results in pronounced difference in the spectra; especially the evolution of the XANES Cu^{I} peak. H_2O-assisted CH_3OH extraction promotes the partial reoxidation of Cu^{I} to Cu^{II} ions as well as the increase in average coordination number evident by the increased WL intensity of XANES. The productivity during the XAS measurements was substantially lower (13 $\mu mol_{CH3OH}/g_{zeolite}$) with respect to the fixed bed reactor conditions indicating the positive effect of prolonged O_2 activation and CH_4 loading on the yield. LCF analysis indicates that during CH_4 loading the amount of formed Cu^{I} accounts for 18% of total Cu while the rest remains as $Cu^{II}fw$. During steam introduction, 5% of Cu^{I} is hydrolyzed which is correlated with the productivity of 0.044 mol_{CH3OH}/mol_{Cu}, suggesting a possible link between these re-oxidized species to the active sites for the selective conversion of CH_4 to CH_3OH.

References

1. Ravi M, Ranocchiari M, van Bokhoven JA (2017) The direct catalytic oxidation of methane to methanol - A critical assessment. Angew Chem Int Ed 56(52):16464-16483
2. Saha D, Grappe HA, Chakraborty A, Orkoulas G (2016) Postextraction separation, on-board storage, and catalytic conversion of methane in natural gas: A review. Chem Rev 116(19):11436-11499
3. Schwach P, Pan X, Bao X (2017) Direct conversion of methane to value-added chemicals over heterogeneous catalysts: Challenges and prospects. Chem Rev 117(13):8497-8520
4. Wang B, Albarracín-Suazo S, Pagán-Torres Y, Nikolla E (2017) Advances in methane conversion processes. Catal Today 285:147-158
5. Groothaert MH, Smeets PJ, Sels BF, Jacobs PA, Schoonheydt RA (2005) Selective oxidation of methane by the bis(μ-oxo)dicopper core stabilized on ZSM-5 and mordenite zeolites. J Am Chem Soc 127(5):1394-1395
6. Sushkevich VL, Palagin D, Ranocchiari M, van Bokhoven JA (2017) Selective anaerobic oxidation of methane enables direct synthesis of methanol. 356(6337):523-527
7. Tomkins P, Mansouri A, Bozbag SE, Krumeich F, Park MB, Alayon EM, Ranocchiari M, van Bokhoven JA (2016) Isothermal cyclic conversion of methane into methanol over copper-exchanged zeolite at low temperature. Angew Chem Int Ed 55(18):5467-5471
8. Tomkins P, Ranocchiari M, van Bokhoven JA (2017) Direct conversion of methane to methanol under mild conditions over Cu-Zeolites and beyond. Acc Chem Res 50(2):418-425
9. Knorpp AJ, Newton MA, Pinar AB, van Bokhoven JA (2018) Conversion of methane to methanol on copper mordenite: Redox mechanism of isothermal and high-temperature-activation procedures. Ind Eng Chem Res 57(36):12036-12039
10. Sheppard T, Hamill CD, Goguet A, Rooney DW, Thompson JM (2014) A low temperature, isothermal gas-phase system for conversion of methane to methanol over Cu-ZSM-5. Chem Commun 50(75):11053-11055
11. Narsimhan K, Iyoki K, Dinh K, Roman-Leshkov Y (2016) Catalytic oxidation of methane into methanol over copper-exchanged zeolites with oxygen at low temperature. ACS Cent Sci 2(6):424-429
12. Ipek B, Lobo RF (2016) Catalytic conversion of methane to methanol on Cu-SSZ-13 using N_2O as oxidant. Chem Commun 52(91):13401-13404
13. J. Smeets P, H. Groothaert M, A. Schoonheydt R (2005) Cu based zeolites: A UV–vis study of the active site in the selective methane oxidation at low temperatures. Catal Today 110:303-309
14. Alayon EM, Nachtegaal M, Ranocchiari M, van Bokhoven JA (2012) Catalytic conversion of methane to methanol over Cu-mordenite. Chem Commun 48(3):404-406
15. Alayon EMC, Nachtegaal M, Kleymenov E, van Bokhoven JA (2013) Determination of the electronic and geometric structure of Cu sites during methane conversion over Cu-MOR with X-ray absorption spectroscopy. Micropor Mesopor Mat 166:131-136
16. Alayon EMC, Nachtegaal M, Bodi A, van Bokhoven JA (2014) Reaction conditions of methane-to-methanol conversion affect the structure of active copper sites. ACS Catal 4(1):16-22
17. Alayon EM, Nachtegaal M, Bodi A, Ranocchiari M, van Bokhoven JA (2015) Bis(μ-oxo) versus mono(μ-oxo)dicopper cores in a zeolite for converting methane to methanol: an in situ XAS and DFT investigation. Phys Chem Chem Phys 17(12):7681-7693
18. Grundner S, Markovits MAC, Li G, Tromp M, Pidko EA, Hensen EJM, Jentys A, Sanchez-Sanchez M, Lercher JA (2015) Single-site trinuclear copper oxygen clusters in mordenite for selective conversion of methane to methanol. 6:7546
19. Grundner S, Luo W, Sanchez-Sanchez M, Lercher JA (2016) Synthesis of single-site copper catalysts for methane partial oxidation. Chem Commun 52(12):2553-2556
20. Vanelderen P, Snyder BE, Tsai ML, Hadt RG, Vancauwenbergh J, Coussens O, Schoonheydt RA, Sels BF, Solomon EI (2015) Spectroscopic definition of the copper active sites in mordenite: selective methane oxidation. J Am Chem Soc 137(19):6383-6392
21. Bozbag SE, Alayon EMC, Pecháček J, Nachtegaal M, Ranocchiari M, van Bokhoven JA (2016) Methane to methanol over copper mordenite: yield improvement through multiple cycles and different synthesis techniques. Catal Sci Tech 6(13):5011-5022
22. Kim Y, Kim TY, Lee H, Yi J (2017) Distinct activation of Cu-MOR for direct oxidation of methane to methanol. Chem Commun 53(29):4116-4119
23. Sushkevich VL, van Bokhoven JA (2018) Effect of Brønsted acid sites on the direct conversion of methane into methanol over copper-exchanged mordenite. Catal Sci Tech 8(16):4141-4150

24. Borfecchia E, Pappas DK, Dyballa M, Lomachenko KA, Negri C, Signorile M, Berlier G (2018) Evolution of active sites during selective oxidation of methane to methanol over Cu-CHA and Cu-MOR zeolites as monitored by operando XAS. Catal Today https://doi.org/10.1016/j.cattod.2018.07.028
25. Newton MA, Knorpp AJ, Pinar AB, Sushkevich VL, Palagin D, van Bokhoven JA (2018) On the mechanism underlying the direct conversion of methane to methanol by copper hosted in zeolites; Braiding Cu K-edge XANES and reactivity studies. J Am Che Soc 140(32):10090-10093
26. Sushkevich VL, Palagin D, van Bokhoven JA (2018) The effect of the active-site structure on the activity of copper mordenite in the aerobic and anaerobic conversion of methane into methanol. Angew Chem Int Ed 57(29):8906-8910
27. Lomachenko KA, Martini A, Pappas DK, Negri C, Dyballa M, Berlier G, Bordiga S, Lamberti C, Olsbye U, Svelle S, Beato P, Borfecchia E (2019) The impact of reaction conditions and material composition on the stepwise methane to methanol conversion over Cu-MOR: an *operando* XAS study. Catal Today https://doi.org/10.1016/j.cattod.2019.01.040
28. Pappas DK, Martini A, Dyballa M, Kvande K, Teketel S, Lomachenko KA, Baran R, Glatzel P, Arstad B, Berlier G, Lamberti C, Bordiga S, Olsbye U, Svelle S, Beato P, Borfecchia E (2018) The nuclearity of the active site for methane to methanol conversion in Cu-mordenite: A quantitative assessment. 140(45):15270-15278
29. Dyballa M, Pappas DK, Kvande K, Borfecchia E, Arstad B, Beato P, Olsbye U, Svelle S (2019) On how copper mordenite properties govern the framework stability and activity in the methane-to-methanol conversion. 9(1):365-375
30. Pappas DK, Borfecchia E, Dyballa M, Pankin IA, Lomachenko KA, Martini A, Signorile M, Teketel S, Arstad B, Berlier G, Lamberti C, Bordiga S, Olsbye U, Lillerud KP, Svelle S, Beato P (2017) Methane to methanol: Structure-activity relationships for Cu-CHA. J Am Chem Soc 139(42):14961-14975
31. Wulfers MJ, Teketel S, Ipek B, Lobo RF (2015) Conversion of methane to methanol on copper-containing small-pore zeolites and zeotypes. Chem Commun 51(21):4447-4450
32. Ipek B, Wulfers MJ, Kim H, Göltl F, Hermans I, Smith JP, Booksh KS, Brown CM, Lobo RF (2017) Formation of $[Cu_2O_2]^{2+}$ and $[Cu_2O]^{2+}$ toward C–H bond activation in Cu-SSZ-13 and Cu-SSZ-39. ACS Catal 7(7):4291-4303
33. Oord R, Schmidt JE, Weckhuysen BM (2018) Methane-to-methanol conversion over zeolite Cu-SSZ-13, and its comparison with the selective catalytic reduction of NO_x with NH_3. Catal Sci Tech 8(4):1028-1038
34. Park MB, Ahn SH, Mansouri A, Ranocchiari M, van Bokhoven JA (2017) Comparative study of diverse copper zeolites for the conversion of methane into methanol. ChemCatChem 9(19):3705-3713
35. Borfecchia E, Beato P, Svelle S, Olsbye U, Lamberti C, Bordiga S (2018) Cu-CHA - a model system for applied selective redox catalysis. Chem Soc Rev 47:8097-8133
36. Smeets PJ, Groothaert MH, Schoonheydt RA (2005) Cu based zeolites: A UV–vis study of the active site in the selective methane oxidation at low temperatures. Catal Lett 110(3-4):303-309
37. Woertink JS, Smeets PJ, Groothaert MH, Vance MA, Sels BF, Schoonheydt RA, Solomon EI (2009) A $[Cu_2O]^{2+}$ core in Cu-ZSM-5, the active site in the oxidation of methane to methanol. Proc Natl Acad Sci USA 106(45):18908-18913
38. Beznis NV, Weckhuysen BM, Bitter JH (2010) Cu-ZSM-5 zeolites for the formation of methanol from methane and oxygen: Probing the active sites and spectator species. Catal Lett 138(1-2):14-22
39. Smeets PJ, Hadt RG, Woertink JS, Vanelderen P, Schoonheydt RA, Sels BF, Solomon EI (2010) Oxygen precursor to the reactive intermediate in methanol synthesis by Cu-ZSM-5. J Am Chem Soc 132(42):14736-14738
40. Vanelderen P, Hadt RG, Smeets PJ, Solomon EI, Schoonheydt RA, Sels BF (2011) Cu-ZSM-5: A biomimetic inorganic model for methane oxidation. J Catal 284(2):157-164
41. Markovits MAC, Jentys A, Tromp M, Sanchez-Sanchez M, Lercher JA (2016) Effect of location and distribution of Al sites in ZSM-5 on the formation of Cu-oxo clusters active for direct conversion of methane to methanol. Top Catal 59(17-18):1554-1563
42. Kulkarni AR, Zhao Z-J, Siahrostami S, Nørskov JK, Studt F (2016) Monocopper active site for partial methane oxidation in Cu-exchanged 8MR zeolites. ACS Catal 6(10):6531-6536
43. Vilella L, Studt F (2016) The stability of copper oxo species in zeolite frameworks. Eur J Inorg Chem 2016(10):1514-1520

44. Zhao Z-J, Kulkarni A, Vilella L, Nørskov JK, Studt F (2016) Theoretical insights into the selective oxidation of methane to methanol in copper-exchanged mordenite. ACS Catal 6(6):3760-3766

45. Mahyuddin MH, Staykov A, Shiota Y, Miyanishi M, Yoshizawa K (2017) Roles of zeolite confinement and Cu–O–Cu angle on the direct conversion of methane to methanol by $[Cu_2(\mu\text{-}O)]^{2+}$-exchanged AEI, CHA, AFX, and MFI zeolites. ACS Catal 7(6):3741-3751

46. Mahyuddin MH, Tanaka T, Shiota Y, Staykov A, Yoshizawa K (2018) Methane partial oxidation over $[Cu_2(\mu\text{-}O)]^{2+}$ and $[Cu_3(\mu\text{-}O)_3]^{2+}$ active species in large-pore zeolites. ACS Catal 8(2):1500-1509

47. Snyder BER, Vanelderen P, Schoonheydt RA, Sels BF, Solomon EI (2018) Second-sphere effects on methane hydroxylation in Cu-zeolites. J Am Chem Soc 140(29):9236-9243

48. Li G, Vassilev P, Sanchez-Sanchez M, Lercher JA, Hensen EJM, Pidko EA (2016) Stability and reactivity of copper oxo-clusters in ZSM-5 zeolite for selective methane oxidation to methanol. J Catal 338:305-312

49. Vogiatzis KD, Li G, Hensen EJM, Gagliardi L, Pidko EA (2017) Electronic structure of the $[Cu_3(\mu\text{-}O)]^{2+}$ cluster in mordenite zeolite and its effects on the methane to methanol oxidation. J Phys Chem C 121(40):22295-22302

50. Palagin D, Knorpp AJ, Pinar AB, Ranocchiari M, van Bokhoven JA (2017) Assessing the relative stability of copper oxide clusters as active sites of a CuMOR zeolite for methane to methanol conversion: size matters? Nanoscale 9(3):1144-1153

51. Pappas DK, Borfecchia E, Dyballa M, Lomachenko KA, Martini A, Berlier G, Arstad B, Lamberti C, Bordiga S, Olsbye U, Svelle S, Beato P (2018) Understanding and optimizing the performance of Cu-FER for the direct CH_4 to CH_3OH conversion. 11(1):621-627

52. Attfield MP, Weigel SJ, Cheetham AK (1997) On the nature of nonframework cations in a zeolitic $deNO_x$ catalyst - A synchrotron X-ray diffraction and ESR study of Cu-ferrierite. J Catal 172(2):274-280

53. Bulanek R, Wichterlova B, Sobalik Z, Tichy J (2001) Reducibility and oxidation activity of Cu ions in zeolites - Effect of Cu ion coordination and zeolite framework composition. Appl Catal, B 31(1):13-25

54. Nachtigall P, Davidova M, Nachtigallova D (2001) Computational study of extraframework Cu^+ sites in ferrierite: structure, coordination, and photoluminescence spectra. J Phys Chem B 105(17):3510-3517

55. Bulanek R, Frolich K, Cicmanec P, Nachtigallova D, Pulido A, Nachtigall P (2011) Combined experimental and theoretical investigations of heterogeneous dual cation sites in Cu,M-FER zeolites. J Phys Chem C 115(27):13312-13321

56. Sklenak S, Andrikopoulos PC, Whittleton SR, Jirglova H, Sazama P, Benco L, Bucko T, Hafner J, Sobalik Z (2013) Effect of the Al siting on the structure of Co(II) and Cu(II) cationic sites in ferrierite. A periodic DFT molecular dynamics and FTIR study. J Phys Chem C 117(8):3958-3968

57. Bordiga S, Groppo E, Agostini G, van Bokhoven JA, Lamberti C (2013) Reactivity of surface species in heterogeneous catalysts probed by in situ X-ray absorption techniques. Chem Rev 113(3):1736-1850

58. Rehr JJ, Albers RC (2000) Theoretical approaches to x-ray absorption fine structure. Rev Mod Phys 72(3):621-654

59. Garino C, Borfecchia E, Gobetto R, van Bokhoven JA, Lamberti C (2014) Determination of the electronic and structural configuration of coordination compounds by synchrotron-radiation techniques. Coord Chem Rev 277-278:130-186

60. Van Bokhoven JA, Lamberti C (2016) X-ray absorption and x-ray emission spectroscopy: Theory and applications. Wiley & Sons, Chichester (UK)

61. Brunauer S, Emmett PH, Teller E (1938) Adsorption of gases in multimolecular layers. J Am Chem Soc 60(2):309-319

62. Abdala PM, Safonova OV, Wiker G, van Beek W, Emerich H, van Bokhoven JA, Sá J, Szlachetko J, Nachtegaal M (2012) Scientific opportunities for heterogeneous catalysis research at the SuperXAS and SNBL beam lines. CHIMIA 66(9):699-705

63. Ravel B, Newville M (2005) ATHENA, ARTEMIS, HEPHAESTUS: data analysis for X-ray absorption spectroscopy using IFEFFIT. J Synchrotron Radiat 12:537-541

64. Lamberti C, Bordiga S, Bonino F, Prestipino C, Berlier G, Capello L, D'Acapito F, Llabrés i Xamena FX, Zecchina A (2003) Determination of the oxidation and coordination state of copper on different Cu-based catalysts by XANES spectroscopy in situ or in operando conditions. Phys Chem Chem Phys 5(20):4502-4509

65. Le Toquin R, Paulus W, Cousson A, Prestipino C, Lamberti C (2006) Time-resolved *in situ* studies of oxygen intercalation into $SrCoO_{2.5}$, performed by neutron diffraction and X-ray absorption spectroscopy. J Am Chem Soc 128(40):13161-13174

66. Lomachenko KA, Borfecchia E, Negri C, Berlier G, Lamberti C, Beato P, Falsig H, Bordiga S (2016) The Cu-CHA deNO-$_x$ catalyst in action: Temperature-dependent NH_3-assisted selective catalytic reduction monitored by *operando* XAS and XES. J Am Chem Soc 138(37):12025-12028

67. Martini A, Borfecchia E, Lomachenko KA, Pankin IA, Negri C, Berlier G, Beato P, Falsig H, Bordiga S, Lamberti C (2017) Composition-driven Cu-speciation and reducibility in Cu-CHA zeolite catalysts: a multivariate XAS/FTIR approach to complexity. Chem Sci 8(10):6836-6851

68. Borfecchia E, Lomachenko KA, Giordanino F, Falsig H, Beato P, Soldatov AV, Bordiga S, Lamberti C (2015) Revisiting the nature of Cu sites in the activated Cu-SSZ-13 catalyst for SCR reaction. Chem Sci 6(1):548-563

69. Giordanino F, Borfecchia E, Lomachenko KA, Lazzarini A, Agostini G, Gallo E, Soldatov AV, Beato P, Bordiga S, Lamberti C (2014) Interaction of NH_3 with Cu-SSZ-13 catalyst: A complementary FTIR, XANES, and XES study. J Phys Chem Lett 5(9):1552-1559

70. Turnes Palomino G, Fisicaro P, Bordiga S, Zecchina A, Giamello E, Lamberti C (2000) Oxidation states of copper ions in ZSM-5 zeolites. A multitechnique investigation. J Phys Chem B 104(17):4064-4073

71. Llabrés i Xamena FX, Fisicaro P, Berlier G, Zecchina A, Palomino GT, Prestipino C, Bordiga S, Giamello E, Lamberti C (2003) Thermal reduction of Cu^{2+}-mordenite and re-oxidation upon interaction with H_2O, O_2, and NO. J Phys Chem B 107(29):7036-7044

72. Mathon O, Beteva A, Borrel J, Bugnazet D, Gatla S, Hino R, Kantor I, Mairs T, Munoz M, Pasternak S, Perrin F, Pascarelli S (2015) The time-resolved and extreme conditions XAS (TEXAS) facility at the European Synchrotron Radiation Facility: the general-purpose EXAFS bending-magnet beamline BM23. J Synchrotron Radiat 22(6):1548-1554

73. Bourgeat-Lami E, Massiani P, Di Renzo F, Espiau P, Fajula F, Des Courières T (1991) Study of the state of aluminium in zeolite-β. App Catal 72(1):139-152

74. Kiricsi I, Flego C, Pazzuconi G, Parker WO, Jr., Millini R, Perego C, Bellussi G (1994) Progress toward understanding zeolite .beta. acidity: An IR and ^{27}Al NMR spectroscopic study. J Phys Chem 98(17):4627-4634

75. Agostini G, Lamberti C, Palin L, Milanesio M, Danilina N, Xu B, Janousch M, van Bokhoven JA (2010) *In Situ* XAS and XRPD parametric rietveld refinement to understand dealumination of Y zeolite catalyst. J Am Chem Soc 132(2):667-678

76. Kwak JH, Tran D, Burton SD, Szanyi J, Lee JH, Peden CHF (2012) Effects of hydrothermal aging on NH_3-SCR reaction over Cu/zeolites. J Catal 287:203-209

77. Engelhard G (1991) Solid State NMR Spectroscopy Applied to Zeolites. In: van Bekkum H, Flanigen EM, Jansen JC (eds) Stud Surf Sci Catal, vol 58. Elsevier, Amsterdam, p 285−315

78. Müller D, Gessner W, Behrens HJ, Scheler G (1981) Determination of the aluminium coordination in aluminium-oxygen compounds by solid-state high-resolution ^{27}AI NMR. 79(1):59-62

79. Narsimhan K, Michaelis VK, Mathies G, Gunther WR, Griffin RG, Roman-Leshkov Y (2015) Methane to acetic acid over Cu-exchanged zeolites: mechanistic insights from a site-specific carbonylation reaction. J Am Chem Soc 137(5):1825-1832

80. Paolucci C, Parekh AA, Khurana I, Di Iorio JR, Li H, Caballero JDA, Shih AJ, Anggara T, Delgass WN, Miller JT, Ribeiro FH, Gounder R, Schneider WF (2016) Catalysis in a cage: condition-dependent speciation and dynamics of exchanged Cu cations in SSZ-13 zeolites. J Am Chem Soc 138(18):6028-6048

81. Prestipino C, Berlier G, Llabrés i Xamena FX, Spoto G, Bordiga S, Zecchina A, Turnes Palomino G, Yamamoto T, Lamberti C (2002) An in situ temperature dependent IR, EPR and high resolution XANES study on the NO/Cu^+-ZSM-5 interaction. Chem Phys Lett 363(3):389-396

82. Sushkevich VL, van Bokhoven JA (2018) Revisiting copper reduction in zeolites: the impact of autoreduction and sample synthesis procedure. Chem Commun 54(54):7447-7450